Multimode waveguide speckle patterns for compressive sensing

GEORGE C. VALLEY,* GEORGE A. SEFLER, T. JUSTIN SHAW

[1]*The Aerospace Corp., 2310 E. El Segundo Blvd. El Segundo, CA 90245-4609*
**Corresponding author: george.valley@aero.org*

Received XX Month XXXX; revised XX Month, XXXX; accepted XX Month XXXX; posted XX Month XXXX (Doc. ID XXXXX); published XX Month XXXX

Compressive sensing (CS) of sparse GHz-band RF signals using microwave photonics may achieve better performance with smaller size, weight and power requirements than electronic CS systems or conventional Nyquist rate sampling systems. The critical element in a microwave photonic CS system is the device that produces the CS measurement matrix (MM). Here we show that passive speckle patterns in multimode fibers or planar waveguides potentially provide excellent MMs for CS. We measure and calculate the MM for a multimode fiber and perform simulations using this MM in a CS system. We show that the speckle MM exhibits the sharp phase transition and coherence properties needed for CS and that these properties are similar to those of a subgaussian MM with the same mean and standard deviation. We calculate the MM for a multimode planar waveguide and find dimensions of the planar guide that give a speckle MM with performance similar to that of the multimode fiber. CS simulations show that all measured and calculated speckle MMs exhibit robust performance with equal amplitude signals that are sparse in time (identity transform), in frequency (discrete cosine transform), and in wavelets (Haar wavelet transform). The planar waveguide results indicate a path to a microwave photonic integrated circuit for measuring sparse GHz-band RF signals using CS.

OCIS codes: (320.7085) Ultrafast information processing; Data processing by optical means; (060.2360) Fiber optics links and subsystems; (250.4745) Optical processing devices

http://dx.doi.org/10.1364/OL.99.099999

High resolution, Nyquist rate sampling of GHz-band RF signals rapidly generates huge amounts of data. Compressive sensing (CS) has been developed to address this general issue for sparse signals and images [1-3]. In CS systems, a sparse input signal x (dimension N) is recovered from a measurement vector y (dimension M) with $M<<N$. The vector y is obtained from x after multiplication by a measurement matrix Φ as in Eq. (1),

$$y = \Phi x = \Phi\Psi^{-1} s \qquad (1)$$

where $s = \Psi x$ is a sparse vector with a small number K of non-zero elements and Ψ is the transform that shows the sparsity of x. If the measurement matrix (MM) Φ satisfies certain properties [1-3], sparse x can be recovered by a range of algorithms provided that M is somewhat greater than K [1,3]. The MM Φ and the matrix multiplication are performed in the analog domain, and an important issue for CS systems is finding a practical way to do this. Since CS recovery calculations require accurate knowledge of Φ [16], it is also mandatory that Φ be reproducible and amenable to calibration.

Both electronic [4,5] and microwave photonic CS systems [6-16] have been demonstrated that recover sparse RF signals. In the GHz band, electronic CS systems suffer from the same sources of error as Nyquist rate ADCs, namely timing jitter and amplitude noise. Photonic CS systems have the equivalent of timing jitter and amplitude noise, but in many cases the distortions are static or lower in frequency and thus more amenable to calibration. Previous photonic systems have used pseudo-random bit sequences (PRBS) for the MM and modulated them on optical carriers with light valves [6-8] or optical modulators [9-15]. Here we demonstrate that propagation of an optically chirped signal through a multimode optical fiber or planar waveguide performs the function of a CS MM.

The CS system proposed here in Fig. 1 uses a multimode waveguide to replace the 2D spatial light modulator in earlier work [7, Fig. 1] and performs the function of the pseudo-random bit sequence in the modulated wideband converter [5, Fig. 3]. Pulses from a femtosecond mode-locked laser (MLL) pass though dispersion compensating fiber (DCF) or other dispersive device with dispersion chosen to stretch the pulse to the interpulse time, pass through a Mach-Zehnder modulator (MZM) that impresses the RF signal on the optical intensity, enter a multimode waveguide, and finally are split spatially at the output of the guide and directed to an array of M photodiodes. Integration time constants of the photodiodes are matched to the MLL pulse period, and the electrical signals from the photodiode array are digitized by an array of ADCs clocked to the MLL pulse repetition frequency (PRF). Optical pulse compression, by placing after the MZM a dispersive element of opposite sign to the DCF, can be used to facilitate signal integration [13]. The components on the left and the right of the multimode waveguide are similar to earlier work [6-8], and again we exploit time-wavelength mapping as depicted by the rainbow-colored pulse icons. At the output of the multimode waveguide are formed speckle patterns that vary with wavelength (and hence time via the time-wavelength mapping of the MLL plus DCF combination), and small changes in wavelength can give

completely different patterns after relatively modest propagation distances [17]. For example, Fig. 2 shows speckle patterns at the end of a 1-m long, 105-μm core diameter, 0.22 NA step-index fiber observed at 1539.44 and 1539.52 nm. An optional fiber mode scrambler (Newport Corporation model FM-1) was used near the input end of the fiber to fully excite the fiber modes. Without the mode scrambler, as much as 10 m of multimode fiber would have been required to realize speckle patterns of similar spatial-frequency content. As seen in Fig. 3, wavelength scans at 4 different locations within the output image of the fiber appear random and uncorrelated. Each of these wavelength scans would correspond to a row of the MM Φ, with the sampling in time set by the time-wavelength mapping property. (In generating Fig. 3, speckle pattern images were recorded while sweeping the wavelength of a single-frequency tunable laser. The combination of the camera frame rate and laser sweep rate provided a wavelength resolution of 0.02 nm.)

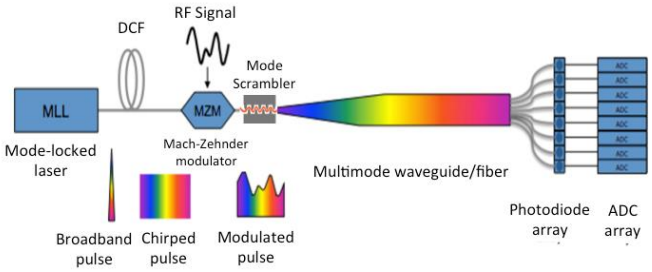

Fig. 1. Compressive sensing system for measuring sparse RF signals using a multimode waveguide to implement the measurement matrix.

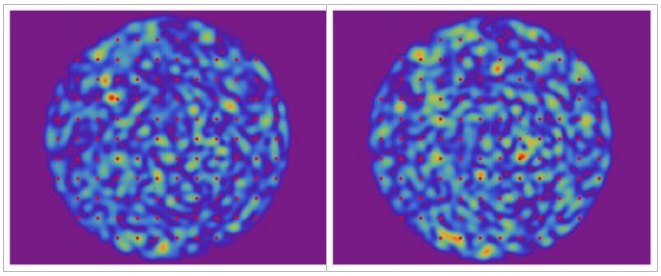

Fig. 2. Speckle patterns at end of 1-m long, 105-μm diameter, 0.22 NA multimode for λ = 1539.44 nm (left) and 1539.52nm (right).

Using the grid of red dots included in Fig. 2, as locations of the output photodiode array, we derive a MM for the multimode fiber from the speckle pattern images as a function of wavelength. For 0.4x0.4 μm apertures, this yields 112 measurements of optical intensity as a function of wavelength, of which 4 are shown in Fig. 3, and a MM with dimensions 112x2048.

We performed several tests to assess whether the measured speckle MM can be used for CS. First, we tried to recover several different types of sparse signals: sparse in time (identity transform, $\Psi = I$), sparse in frequency (discrete cosine transform), and sparse after the Harr wavelet transform. Fig. 4 shows the probabilities that the RF signals are recovered as a function of the small dimension M of the MM. A signal is classified as recovered if all K of its unknown frequencies, pulse locations, or Haar coefficients are recovered and the amplitudes are recovered to better than 1 part in 10,000. For each basis, the sparse vector s consists of K equal-amplitude numbers randomly placed on a 2048-point grid, and each curve is for 100 realizations of the sparse vector s. We used a standard LASSO code [18] to obtain the recovered vector x_{rec}, and we varied the small dimension M of the MM by stripping rows off of the 112x2048 MM. The results are consistent with the well known formula for the minimum dimension of the measurement matrix, $M_{min} \sim K \log(N/K)$ [2,3], and the measured speckle MM works well for signals sparse in all three bases. Note that the pulses with the identity matrix for Ψ ??? recovered somewhat better than the sinusoids (Ψ ?qual the discrete cosine transform) or Haars (Ψ equals the Haar transform matrix). This is caused by the fact that the speckle MM is more correlated with the Haar and cosine basis vectors than with the identity basis.

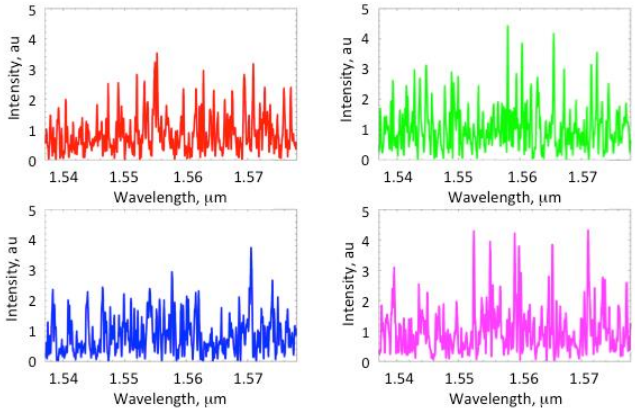

Fig. 3. Measured intensity as a function of wavelength at 4 locations within the output plane of a 1-m, 105-μm, 0.22NA step-index fiber.

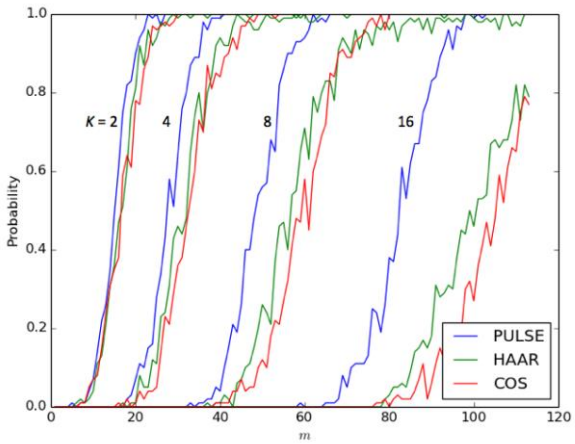

Fig. 4. Probability of signal recovery as a function of small dimension of the measurement matrix for 100 trials for K = 2, 4, 8 and 16 and signals sparse in the identity, discrete cosine and Haar wavelet transforms.

A second test involves the coherence between the rows of the MM Φ, which ideally should be uncorrelated with each other so that each component of y is an independent measurement of the input x [19]. This can be quantified with the normalized mutual coherence C_{ij}

$$C_{ij} = \Phi(i).\Phi(j)/[|\Phi(i)||\Phi(j)|], \qquad (2)$$

for all i, j $(i \neq j)$. Fig. 5 (left) overlays the 12,432 coherences calculated from the 112x2048 measured multimode-fiber speckle MM, and for comparison, Fig. 5 (right) shows the coherences for a MM composed of Gaussian random numbers with the same mean and standard deviation as elements of the speckle MM. The mutual coherence for the measured speckle MM is a bit broader than the random matrix, but the measured MM has very good coherence. (Note many CS MMs use positive and negative numbers as opposed to the positive numbers used here. A MM with positive and negative numbers can be achieved in our speckle system by subtracting photodiode signals from one another as suggested in another context by [11]. Should more photodiode signals be needed to reach M rows, the output of the MZM in Fig. 1 can be split and input into an additional multimode waveguide and photodiode array.)

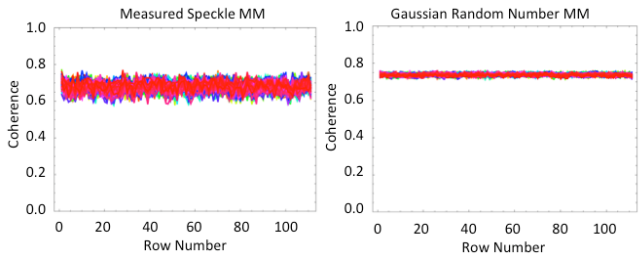

Fig. 5. Mutual coherence between rows for speckle MM (left) and Gaussian random-number MM (right).

A third well-known test for a CS MM is the restricted isometry property (RIP) [1-3]. Unfortunately, proving RIP appears to be computationally intractable. A surrogate to proving RIP suggested by [20] is performing numerical experiments to determine if the MM produces a recovery "phase transition". The "phase transition" is seen as a sharp boundary between regions of high probability of recovery and regions of low probability of recovery in a 3D plot of probability as a function of *M* and *K*. Fig. 6 shows the phase transitions for the multimode-fiber speckle MM and the random MM for signals sparse in time, and the difference is minimal. CS MMs must be equally effective against all possible bases in which an input signal may be sparse, and this occurs when the rows of the MM are uncorrelated with the bases of interest. It is not possible to test all possible bases, but we have also performed CS recovery calculations with signals sparse in cosines and Haars with the results shown in Fig. 7. It can be seen that the measured fiber MM yields very similar sharp phase transitions when used with all three bases.

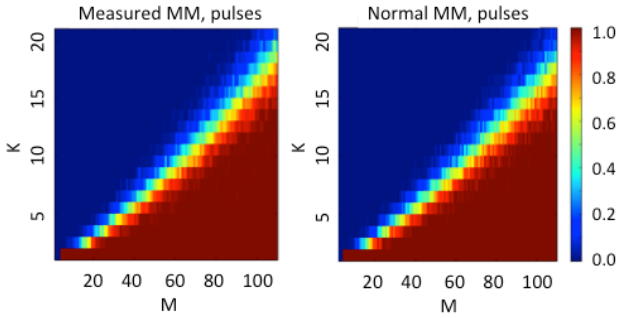

Fig. 6. Probability of recovery as a function of sparsity *K* and number of measurements *M* for the speckle MM (left) and the Gaussian random-number MM (right).

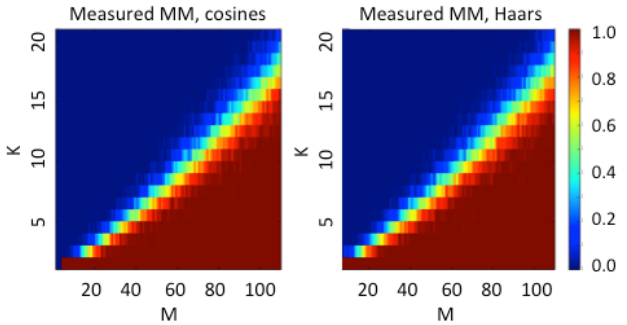

Fig. 7. Probability of recovery as a function of sparsity *K* and the number of measurements *M* for the measured speckle MM with a signal composed of K sinusoids (left) and a signal that is K sparse under the Haar wavelet transform (right).

Analytical solutions for a multimode cylindrical waveguide are well known, and for a weakly guiding fiber as used in our measurements, they reduce to the LP modes [21, 22] in which the TE and TM modes are degenerate. For the parameters of our fiber (core diameter = 105 μm, length = 1 m, NA = 0.22) and for equal power in each mode to approximate the mode-scrambler, we calculate the output intensity at the locations shown by the red dots in Fig. 2. Fig. 8 shows 4 rows of the calculated MM; visually, there is no significant difference from the measured MM rows shown in Fig. 3.

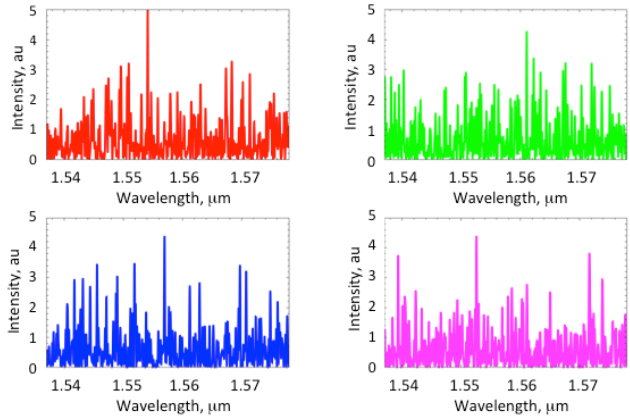

Fig. 8. Calculated intensity as a function of wavelength at 4 locations within the output plane of a 1-m, 105-μm, 0.22NA step-index fiber.

Analytical solutions for a planar multimode waveguide are also well known [22, 23]. We have used these solutions to calculate speckle patterns for planar waveguides and to design a suitable guide for the CS MM. We consider a silicon-on-insulator (SOI) guide which leads to a strongly guiding case in which both TE and TM modes must be considered. We assume that the power per mode is equal at the entrance to the guide and recognize that achieving this in practice will require use of a mode-scrambling technique. First, to determine the width of the guide, we examine speckle patterns such as shown in Fig. 9 for a 10cm guide. From Fig. 9, one can see that the 5μm wide guide has only 10 to 15 speckle lobes, and this would limit M to less than around 30 if it were used as a CS MM. A guide between 20 and 30 μm wide appears to have enough independent spatial locations to support M ~ 100. Fig. 10 shows overlapping speckle patterns at the output of a 25.4-μm wide planar waveguide for 50 wavelengths separated by 0.01nm and for guides 1mm, 1cm, 10cm and 1m long. The 1mm and 1cm guides are clearly not long enough as all 50 wavelength speckle patterns are highly correlated with each other. On the other hand, a planar waveguide 1m long may be impractical. A guide length of 5 to 10 cm appears to be the minimum that will have sufficient mixing for CS.

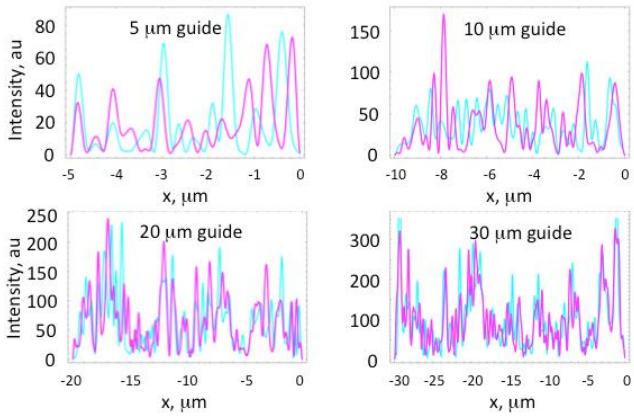

Fig. 9. Speckle patterns at the output of a 10-cm long SOI waveguide for guides 5, 10, 20 and 30 μm wide. The magenta and cyan curves are for wavelengths of λ = 1.537 and 1.53701 μm respectively.

Based on the calculations displayed in Figs. 9 and 10, we chose a waveguide 25.4 mm wide and 5 cm long for comparison with the fiber results. Fig. 11 shows the phase transition plot calculated for the multimode fiber and planar waveguide MM. The planar results are

slightly inferior to the fiber, but it seems likely that optimizing the width and length of the planar guide will yield similar performance.

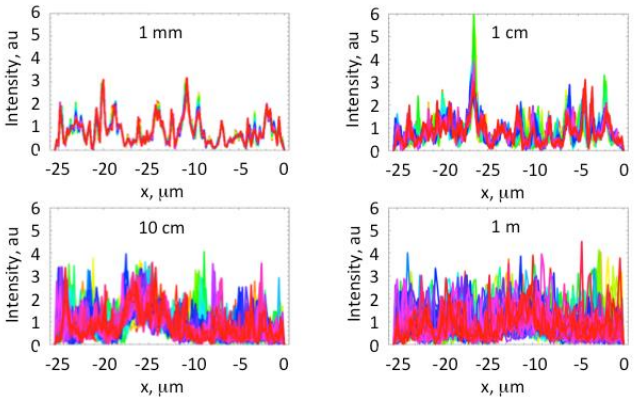

Fig. 10. Speckle patterns across an SOI waveguide for 50 wavelengths separated by 0.01 nm and for guide lengths of 1mm to 1m.

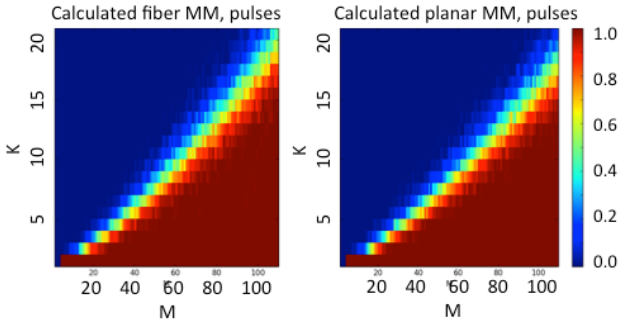

Fig. 11. Probability of recovery as a function of sparsity *K* and the small dimension of the MM *M* for the calculated fiber MM (left) and the calculated planar waveguide MM (right).

Practical use of speckle in a multimode waveguide for CS requires that the speckle MM, the MLL pulse and any other dispersion in the system be stable and amenable to calibration. Previous work [7, 8, 13, 14] has found that commercial mode-locked lasers were sufficiently stable for CS. The stability of speckle from a multimode waveguide depends on control of temperature and mechanical stresses (e.g., bending of the fiber). In our laboratory measurements with the multimode fiber, basic precautions were taken to ensure stable speckle patterns, namely securing the fiber from perturbations; these steps are similar to those routinely taken to obtain stable polarizations within non-polarization-maintaining singlemode fiber. Fig. 12 shows the match between two wavelength calibrations taken more than 1 hour apart (using a tunable single-frequency laser) for a single row of a MM obtained with a single photodiode placed in the image plane of the multimode fiber output. Other work using speckle in a similar 1m, 105μm, 0.22NA multimode fiber for spectroscopic applications discusses stability of the speckle pattern in detail [17, Sections 8 and 9]. For example, [17] states that "for a 1 m long fiber, the temperature would need to change by ~8°C to decorrelate the speckle pattern."

A potential factor limiting the RF bandwidth of a speckle-based CS system is that the frequency content of the RF signal itself may modify the speckle pattern. At an optical wavelength of 1550nm, should the speckle pattern vary on a 0.05 nm wavelength scale, the MM will be frequency dependent for RF signals with frequency content above 6.24 GHz. However, the speckle MM can still be used for CS if the system is calibrated by measuring the response for all basis vectors in which the RF signal is sparse. Referring to Eq. 1, the calibration consists of measuring y_i for each basis vector *i*. This *M*x*N* matrix, in which *N* is now the number of possible basis vectors in the RF signal, can be used as the dictionary to recover the signal using an orthogonal matching pursuit recovery algorithm [8]. The variation of the speckle MM with

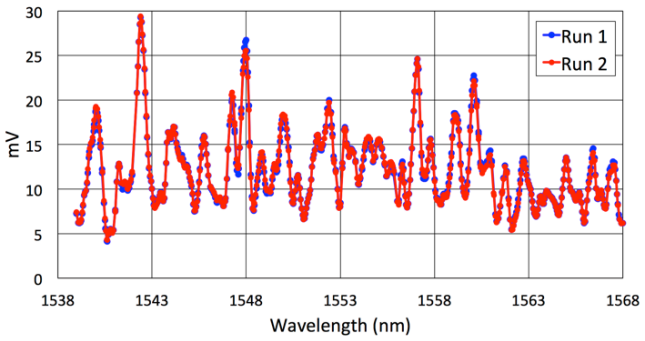

Fig. 12. Two independent calibrations of the multimode fiber separated in time by more than 1 hour.

RF frequency suggests that it may be possible to measure RF signals modulated on a stable single-frequency laser directly from the change in speckle pattern, a subject for future investigation.

To conclude, we show that optical speckle in multimode fibers and planar waveguides satisfies 3 tests for a compressive sensing measurement matrix: 1) CS simulations show expected recovery as a function of the number of measurements, 2) rows of the speckle MMs show coherence properties similar to a MM formed from Gaussian random numbers, and 3) recovery plotted in the sparsity/measurement plane (K-M) shows sharp phase transitions for all measured and calculated speckle MMs and for 3 classes of sparse signals. The next step is to couple an array of photodiodes and ADCs to the output of the multimode guide and demonstrate a full CS system.

References

1. D. L. Donoho, IEEE Trans. Inf. Theory **52**, 1289 (2006)
2. E. J. Candès and M. B. Wakin, IEEE Signal Process. Mag. **25**, 21 (2008).
3. R. G. Baraniuk, IEEE Signal Process. Mag. **24**, 118 (2007).
4. J. A. Tropp, J. N. Laska, M. F. Duarte, J. K. Romberg, and R. G. Baraniuk, IEEE Trans. Inf. Theory **56**, 520 (2010).
5. M. Mishali and Y. Eldar, IEEE J. Sel. Top. Signal Process. **4**, 375 (2010).
6. G. C.Valley and G. A. Sefler, Proc. SPIE **7797**-14, (2010).
7. G. C. Valley G. A. Sefler, and T. J. Shaw, Opt. Lett. **37**, 4675 (2012).
8. G. C. Valley, G. A. Sefler and T. J. Shaw, Proc. SPIE **8645** 86450P-1 (2013).
9. H. Nan, Y. Gu, and H. Zhang, IEEE Photonics Tech. Lett. **23**, 67 (2011).
10. J. M. Nichols and F. Bucholtz, Opt. Express **19**, 7339 (2011).
11. H. Chi, Y. Mei, Y. Chen, D. Wang, S. Zheng, X. Jin, and X. Zhang, Opt. Lett. **37**, 4636 (2012).
12. H. Chi, Y. Chen, Y. Jei, X. Jin, S. Zheng, and X. Zhang, Opt. Lett. **38**, 136-138, (2013).
13. B. T. Bosworth and M. A. Foster, Opt. Lett. **38**, 4892 (2013).
14. B. T. Bosworth, J. R. Stroud, D. N. Tran, T.D. Tran, S. Chin, and M. A. Foster, Opt. Lett. **40**, 3045 (2015)
15. Y. Chen, X. Yu, H. Chi, S. Zheng, X. Zhang, X. Jin, and M. Galili, Opt. Commun. **338**, 428 (2015).
16. J. T. Parker, V. Cevher, and P. Schniter, Conference Record of the Forty Fifth Asilomar Conference on Signals, Systems and Computers (ASILOMAR), IEEE, pp. 804-808 (2011).
17. B. Redding, S. M. Popoff, and H. Cao, Optics Express **21**, 6584 (2013).
18. I. Loris, Computer Physics Communications, **179**, 895 (2008). We also used Section 1.1.3 "Lasso" at http://scikit-learn.org/stable/modules/linear_model.html
19. A. Juditsky, and A. Nemirovski, Mathematical Programming **127**, 57 (2011).
20. D. Donoho and J. Tanner, Philosophical Transactions of the Royal Society of London A: Mathematical, Physical and Engineering Sciences **367**, 4273 (2009).
21. D. Gloge, Appl. Opt. **10**, 2252 (1971).
22. D. Marcuse, Theory of Dielectric Waveguides (Academic Press 1974).
23. A. Yariv, IEEE J. Quantum Electronics **QE-9**, 919-933 (1973)

1. D. L. Donoho, “Compressed sensing,” IEEE Trans. Inf. Theory, **52**, 1289 (2006)
2. E. J. Candès and M. B. Wakin. "An introduction to compressive sampling", *IEEE Signal Processing Magazine,* **25**, 21-30 (2008).
3. R. G. Baraniuk, “Compressive sensing,” *IEEE Signal Processing Magazine,* **24**, 118,(2007).
4. J. A. Tropp, J. N. Laska, M. F. Duarte, J. K. Romberg, and R. G. Baraniuk, “Beyond Nyquist: Efficient sampling of sparse bandlimited signals,” IEEE Trans. Inf. Theory 56, 520 (2010).
5. M. Mishali and Y. Eldar, “From theory to practice: Sub-Nyquist sampling of sparse wideband analog signals,” IEEE J. Sel. Top. Signal Process. **4**, 375 (2010).
6. G. C. Valley and G. A. Sefler, “Optical time-domain mixer,” Proc. SPIE **7797**-14, (2010).
7. G. C. Valley G. A. Sefler, and T. J. Shaw, "Compressive sensing of sparse RF signals using optical mixing," Opt. Lett. **37**, 4675-4677 (2012).
8. G. C. Valley, G. A. Sefler and T. J. Shaw, “Sensing RF signals with the optical wideband converter,” Proc. SPIE **8645** 86450P-1 (2013).
9. H. Nan, Y. Gu, and H. Zhang, “Optical analog-to-digital conversion system based on compressive sensing,” IEEE Photonics Tech. Lett, **23**, 67-69 (2011).
10. J. M. Nichols and F. Bucholtz, “Beating Nyquist with light: a compressively sampled photonic link,” Opt. Express, **19**, 7339-7348 (2011).
11. H. Chi, Y. Mei, Y. Chen, D. Wang, S. Zheng, X. Jin, and X. Zhang, “Microwave spectral analysis based on photonic compressive sampling with random demodulation,” Opt. Lett. **37**, 4636-4638 (2012).
12. H. Chi, Y. Chen, Y. Jei, X. Jin, S. Zheng, and X. Zhang, “Microwave spectrum sensing based on photonic time stretch and compressive sampling,” Opt. Lett. **38**, 136-138, (2013).
13. B. T. Bosworth and M. A. Foster. "High-speed ultrawideband photonically enabled compressed sensing of sparse radio frequency signals." Opt. Lett. **38**, 4892 (2013).
14. B. T. Bosworth, J. R. Stroud, D. N. Tran, T.D. Tran, S. Chin, and M. A. Foster, "Ultrawideband compressed sensing of arbitrary multi-tone sparse radio frequencies using spectrally encoded ultrafast laser pulses," Opt. Lett. **40**, 3045-3048 (2015).
15. Y. Chen, X. Yu, H. Chi, S. Zheng, X. Zhang, X. Jin, and M. Galili, “Compressive sensing with a microwave photonic filter,” Opt. Commun. **338**, 428 (2015).
16. J. T. Parker, V. Cevher, and P. Schniter. "Compressive sensing under matrix uncertainties: An approximate message passing approach." *Conference Record of the Forty Fifth Asilomar Conference on Signals, Systems and Computers (ASILOMAR)*, IEEE, pp. 804-808, (2011).
17. B. Redding, S. M. Popoff, and H. Cao. "All-fiber spectrometer based on speckle pattern reconstruction." *Optics express* **21**, 6584-6600, (2013).
18. I. Loris, "L1Packv2: A Mathematica package for minimizing an ℓ1-penalized functional." *Computer physics communications* **179**, 895-902 (2008). We also used Section 1.1.3 “Lasso” at http://scikit-learn.org/stable/modules/linear_model.html
19. A. Juditsky, and A. Nemirovski, "On verifiable sufficient conditions for sparse signal recovery via ℓ 1 minimization." *Mathematical programming* **127**, 57-88 (2011).
20. D. Donoho and J. Tanner, "Observed universality of phase transitions in high-dimensional geometry, with implications for modern data analysis and signal processing." *Philosophical Transactions of the Royal Society of London A: Mathematical, Physical and Engineering Sciences* **367**, 4273-4293 (2009).
21. D. Gloge, “Weakly guiding fibers,” Appl. Opt. **10**, 2252 (1971).
22. D. Marcuse, Theory of Dielectric Waveguides (Academic Press 1974).
23. A. Yariv, “Coupled-mode theory for guided-wave optics.” IEEE J. Quantum Electronics **QE-9**, 919-933 (1973).